Energy harvesting with vortex induced vibrations

Sundarram Datla
University of Wisconsin-Madison
sdatla@wisc.edu

November 23 2025

ABSTRACT
Traditional methods of utilizing water currents such as hydropower turbines rely on high flow velocity. This excludes the implementation of hydropower in many bodies of water, where the flow velocity is regularly too low to justify expensive implementation of hydropower turbines. Thus, the exploration of energy generation methods in low flow velocity is essential to fully unlock the available hydropower on the planet. In this paper, the potential use of vortex induced vibrations of a cylinder created by slow moving currents in harvesting hydropower is explored computationally via Python. The 2-dimensional incompressible Navier-Stokes equation is solved using Chorin's projection method with an in-flow velocity boundary condition and mixed boundary conditions on the outflow. Flow is initialized to have an inflow velocity of 2 knots at a Reynolds number of 100 with a cylinder of radius 0.2 m and mass of 1 kilogram. A direct-forcing immersed boundary method is used to simulate vortex induced vibrations between the cylinder and fluid. Power is generated using electromagnetic induction with a magnet coupled to the cylinder and oscillating in and out of a coil of wire at the vortex shedding frequency. Simulation results show $4.122\mu W$ generated by a singular cylinder. These preliminary findings suggest the potential of vortex induced vibrations in generating power for remote water systems such as sensors and the ability to easily scale power generation by adding more cylinders.

Key words: Vortex induced vibrations, hydropower, energy harvesting

1 INTRODUCTION

The phenomenon of vortex shedding of cylinders is a well known destructive phenomenon that occurs in skyscrapers, bridges, chimneys, and smoke stacks. Flow is detached by the bluff body, creating alternating voritices behind the object known as a "Von Karman street." These vortices create alternating high pressure on the object's transversal sides, leading to periodic lift forces and transversal oscilliatory harmonic motion called vortex induced vibrations (VIV). If the frequency of the VIV reaches the object's fundamental resonance frequency, it can cause catastrophic oscillations that lead to structural collapse in the real world, such as the 1940 Tacoma Narrows bridge collapse. Yet in the same way that a raging water current can induce catastrophic damage to structures, it can also be utilized to generate power through channeling it into a hydropowered turbine. By the same token, the utilization of the destructive force of naturally-occuring vortex induced vibrations to also generate power is of interest to the physicists studying renewable energy sources. Hydropower has a long history of generating clean and reliable energy since antiquity. However, concerns regarding ecological damage and scalability issues need to be addressed. It is well documented that traditional hydroelectric systems create extensive damage to aquatic ecosystems, often significantly reducing wildlife in the very source they are built in. Additionally, traditional hydropower are poorly equipped to transfer low fluid flow into power, which leaves slow moving currents across the world as untapped sources of electricity. For these reasons, scientists have begun to experiment with unobtrusive methods of generating electricity in the low flow regime. One of the most promising methods is utilizing vortex induced vibrations to generate energy and is currently in its novel stages of actualization. The leading experts in this field are researchers at the University of Michigan developing the VIVACE (Vortex Induced Vibrations for Aquatic Clean Energy), which has shown promising results with their latest test in Michigan's St. Clair river in 2016. St. Clair's slow moving current of 3 knots was able to generate on average 1 kilowatt with 4 aluminum cylinders used in the VIVACE system [Ref. 9]. To further these

promising results, this paper's purpose is two fold. The first is to report preliminary results of power generation for a cylinder of radius .2 meters and mass of 1 kg immersed in 2 knots of current. The second is to provide computational methodology for scientists and engineers to accurately simulate vortex induced vibrations for prototyping and educational purposes. To counteract the unwelcoming pedantic nature of current CFD literature, this paper will thoroughly and intuitively explain the methodology and algorithms used to computationally solve the 2D Navier-Stokes equations, simulate VIV through fluid-structure interaction, and calculate voltage output and power generation as a function of vortex shedding frequency.

2 THEORY

Vortex shedding is a phenomenon that appears in fluid flow with a Reynolds number of at least 100 when incoming fluid collides with a bluff body such as a cylinder. This causes the flow to detach and form a turbulent wake behind the bluff body known as a "Von Karman Street." As flow detaches above and below the cylinder, assuming it is oriented horizontally to the flow, a low pressure zone is formed and the body is forced towards it by suction, leading to the effect of vortex induced vibrations.

Our methodology begins by initializing a 5x5 meter domain size with a uniform mesh with N = 161 points and grid spacing of:

$$\texttt{element\_length} = \frac{\texttt{domain\_size}}{\texttt{N} - 1}$$

The center, radius, and mass of the cylinder on the 2D mesh are defined on the mesh at this step. The initial pressure scalar field is 0 Pa at every mesh point. The initial fluid velocity profile is 0 m/s at every point except the left-most column of nodes defined as the inlet with a horizontal velocity u = 1.0 m/s. In order to simulate fluid flow, the horizontal fluid velocity u and vertical fluid velocity v must be time step evolved numerically at each mesh node according to the 2-D incompressible Navier-Stokes equation:

$$\frac{\partial u}{\partial t} + u\frac{\partial u}{\partial x} + v\frac{\partial u}{\partial y} = -\frac{1}{\rho}\frac{\partial p}{\partial x} + \nu\left(\frac{\partial^2 u}{\partial x^2} + \frac{\partial^2 u}{\partial y^2}\right) + f_x, \tag{1}$$

$$\frac{\partial v}{\partial t} + u\frac{\partial v}{\partial x} + v\frac{\partial v}{\partial y} = -\frac{1}{\rho}\frac{\partial p}{\partial y} + \nu\left(\frac{\partial^2 v}{\partial x^2} + \frac{\partial^2 v}{\partial y^2}\right) \tag{2}$$

$$\frac{\partial u}{\partial x} + \frac{\partial v}{\partial y} = 0. \tag{3}$$

The algorithm used in this paper to solve the 2-D Navier Stokes equation is Chorin's projection method. This method is based on the Helmholtz-Hodge decomposition of vector fields into a divergence free and irrotational vector field:

$$\mathbf{w} = \mathbf{w}_{\text{sol}} + \mathbf{w}_{\text{irrot}} = \mathbf{w}_{\text{sol}} + \nabla\phi$$

The divergence-free vector field $\mathbf{w}_{\text{sol}}$ is what we are interested in and can be obtained from

$$\mathbf{w}_{\text{sol}} = \mathbf{w} - \nabla\phi. \tag{4}$$

In order to solve for the solenoidal vector field, the original vector field $\mathbf{w}$ must be solved via the Poisson equation, which is derived by taking the divergence of the original equation:

$$\nabla \cdot \mathbf{w} = \nabla^2\phi. \tag{5}$$

This allows us to turn any vector field $\mathbf{w}$ divergence free simply by subtracting the gradient of the corresponding scalar field. This fact will be used later to prove that the vector field achieved after the operator splitting step is divergence free and thus obeys the conservation of mass requirement of Navier-Stokes.

We can use operator splitting [Ref. 4] to separate the momentum and pressure terms and discretize them:

$$\frac{\mathbf{w}^* - \mathbf{w}^n}{\Delta t} = -(\mathbf{w}^n \cdot \nabla)\mathbf{w}^n + \nu\nabla^2\mathbf{w}^n \tag{6}$$

$$\frac{\mathbf{w}^{n+1} - \mathbf{w}^*}{\Delta t} = -\frac{1}{\rho}\nabla p^{n+1} \tag{7}$$

$\mathbf{w}^n$ is the current fluid velocity field and $\mathbf{w}^*$ is the intermediate fluid velocity field, which does not obey the divergence-free requirement of Navier-Stokes. However, rearranging equation (7) reveals:

$$\mathbf{w}^{n+1} = \mathbf{w}^* - \frac{\Delta t}{\rho}\nabla p^{n+1} \tag{8}$$

By Hemholtz-Hodge Decomposition, $\mathbf{w}^{n+1}$ is divergence-free and thus obeys the conservation of momentum requirement. Taking the divergence of this equation yields us a Poisson equation to solve for the pressure at time step n+1, which is necessary to solve equation (7):

$$\nabla^2 p^{n+1} = \frac{\rho}{\Delta t}\nabla \cdot \mathbf{w}^* \tag{9}$$

The pressure Poisson equation is solved in this paper using Jacobi's iterative method by discretizing the Laplacian and solving for $p_{i,j}$ with 50 iterations:

$$p_{i,j}^{n+1} = \frac{1}{4}\Big(p_{i+1,j}^n + p_{i-1,j}^n + p_{i,j+1}^n + p_{i,j-1}^{n+1} - \frac{\rho h^2}{\Delta t}(\nabla \cdot \mathbf{w}^*)_{i,j}\Big). \tag{10}$$

Thus, the full projection method used to solve the 2-D Navier-Stokes equation is done by first solving the momentum equation (6) by central difference method and applying inflow/outflow boundary conditions on $\mathbf{w}^*$. Then solve the Poisson pressure equation (9) and apply homogeneous Neumann pressure boundary conditions on all sides of the domain except for a 0 Pa Dirichlet boundary condition on the outflow. Lastly, apply this pressure correction to the intermediate velocity in equation (8) and achieve the divergence-free fluid velocity $\mathbf{w}^{n+1}$ and once again apply the fluid velocity boundary conditions.

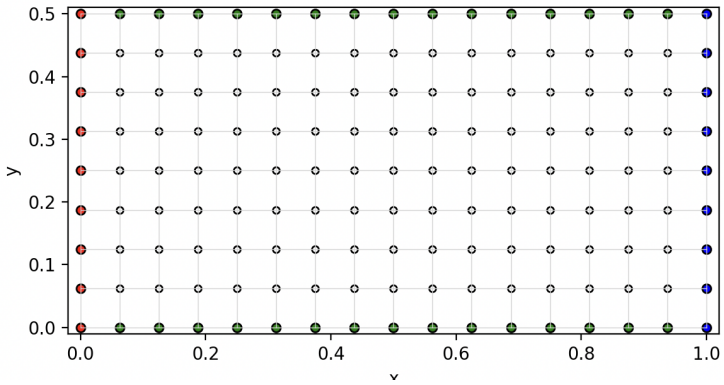

An example of the mesh generated for this paper. To set up boundary conditions, the red nodes are assigned only a horizontal velocity of 1.0 m/s, the fluid velocity at the column of blue nodes are the same as the column to the left of it. The green nodes at the top and bottom of the mesh have fluid flow velocity of 0 m/s.

The next step is to implement fluid-structure interaction between the current flow and cylinder in order to simulate the vortex induced vibrations. The algorithm used to achieve this is the direct-forcing immersed boundary method, which couples with the projection method developed earlier. The idea of this algorithm is to discretize along the boundary surface into nodes, similar to the initial mesh set up. These nodes, called Lagrangian points, are distinguished from the nodes used to define the fluid velocity

on, which are called Eulerian points. This paper has chosen $N_l = 100$. The velocity of the fluid at each of these Lagrange mesh

points must be calculated, along with the force that leaves the boundary slip-free. $\mathbf{w}*$ is explicitly corrected with this force and the structure's position will also be updated using the same force in accordance with Newton's 3rd law. However, one issue that will be inevitably encountered is that the Lagrangian mesh points do not necessarily lie over the Eulerian mesh which was generated earlier:

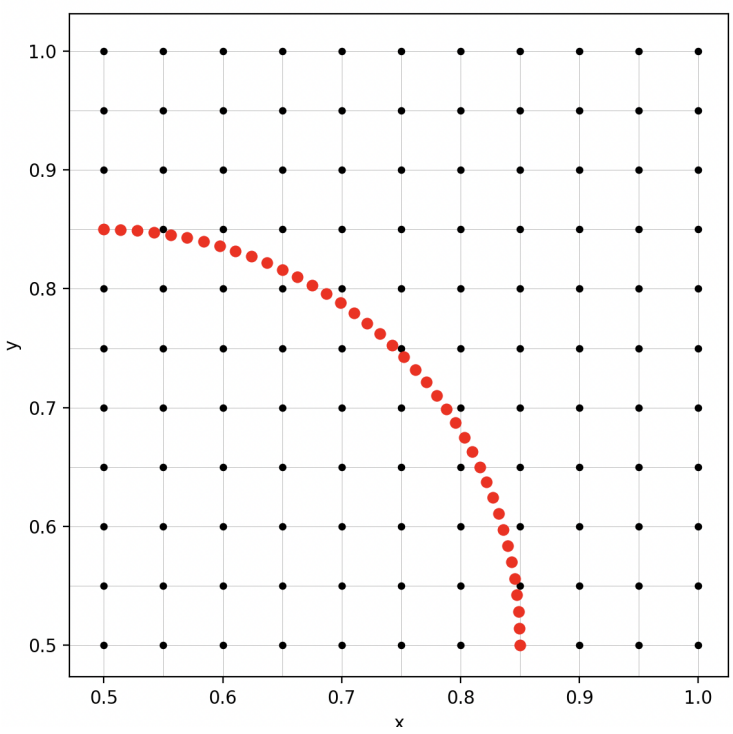

As seen in the plot, the red Lagrangian boundary mesh points do not align with the Eulerian mesh.

This presents the problem that the fluid velocities are unknown at these points outside the discrete Eulerian mesh. However, the IBM method resolves this with a special function that takes the fluid velocity $\mathbf{w}$ of the 4 nearest grid points enclosing the Lagrange mesh point and interpolates a weighted average of those mesh points onto the Lagrangian mesh point as its fluid velocity $\mathbf{W}^*$ [Ref. 6]. Therefore, the fluid velocity at the Eulerian mesh point closest to the Lagrangian mesh point will dominate the weighted average. This special function is a regularized delta function, of which there are many variations that will yield varying levels of accuracy. For this paper, the 4-point Peskin kernel $\phi(r)$ [Ref. 8] is used:

$$\phi(r) = \begin{cases} \frac{1}{8}\left(3 - 2|r| + \sqrt{1 + 4|r| - 4|r|^2}\right), & 0 \le |r| < 1, \\ \frac{1}{8}\left(5 - 2|r| - \sqrt{-7 + 12|r| - 4|r|^2}\right), & 1 \le |r| < 2, \\ 0, & |r| \ge 2. \end{cases} \tag{11}$$

Where $\mathbf{r}$ is the non-dimensional distance measured in units of grid spacing and h is the element length defined earlier. Thus for a

Lagrangian marker at position $\mathbf{X}_l = (X_l, Y_l)$, the fluid velocity at that point $\mathbf{W}^*(\mathbf{X}_l)$ is attained by this interpolation step [Ref. 7]:

$$\mathbf{W}^*(\mathbf{X}_l) = \begin{pmatrix} U^*(\mathbf{X}_l) \\ V^*(\mathbf{X}_l) \end{pmatrix} = \sum_{i,j} \begin{pmatrix} u_{i,j} \\ v_{i,j} \end{pmatrix} \phi\left(\frac{x_i - X_l}{h}\right) \phi\left(\frac{y_j - Y_l}{h}\right), \tag{12}$$

The structure's position evolves according to its own equations of motion. For the cylinder undergoing vortex induced vibrations,

these are the simple 1-D harmonic oscillator in the y direction with velocity $\mathbf{W}_{sho}(\mathbf{X}_l)$ at each Lagrangian mesh point. To enforce the no-slip boundary condition:

$$\mathbf{W_{sho}}(\mathbf{X_l}) = \mathbf{W}^*(\mathbf{X_l}) \tag{13}$$

we must calculate a force at each time step that increases or decreases the fluid's velocity to match the boundary's velocity and append it to $\mathbf{w}*$:

$$\mathbf{F}(\mathbf{X_l}) = \rho \frac{\mathbf{W_{sho}}(\mathbf{X_l}) - \mathbf{W}^*(\mathbf{X_l})}{\Delta t} \tag{14}$$

This calculated force must be distributed out back to the Eulerian mesh points in order to append it to the fluid velocity $\mathbf{w}*$. Thus the 4-point Peskin kernel is used once again to spread this force onto the nearby Eulerian mesh points using the same weighted average philosophy [Ref. 7]:

$$F_x(x_i, y_j) = \sum_{l=1}^{N_L} F_{x,l}\, \phi\left(\frac{x_j - X_l}{h}\right) \phi\left(\frac{y_i - Y_l}{h}\right) \frac{\Delta s_l}{h^2},$$

$$F_y(x_i, y_j) = \sum_{l=1}^{N_L} F_{y,l}\, \phi\left(\frac{x_j - X_l}{h}\right) \phi\left(\frac{y_i - Y_l}{h}\right) \frac{\Delta s_l}{h^2}.$$

where Δs_l is the arc-length that each Lagrange marker represents and is equal to $\Delta s_l = \frac{2\pi R}{N_l}$. Finally, $\mathbf{w}*$ is corrected:

$$\mathbf{w}*(x_i, y_j) = \mathbf{w}*(x_i, y_i) + \frac{\Delta t}{\rho}\mathbf{F}(x_i, y_j) \tag{15}$$

The intermediate fluid's boundary conditions and the remainder of Chorin's projection method are applied. The last step in the direct-forcing IBM method is to update the simple harmonic oscillator equations of motion governing the Lagrange markers. By Newton's 3rd Law, the forcing term for the simple harmonic motion is simply the negative of the total force $F_y(x_i, y_j)$:

$$F_{hy} = -\sum_{i,j} F_y(x_i, y_j)\, h^2 \tag{16}$$

The equations of motions governing the VIV of the cylinder are solved at each time step by a simple semi-implicit Euler method:

$$\ddot{y}^n = \frac{F_{hy}^n - c_{\text{damp}}\, \dot{y}^n - k_{\text{stiff}}\, y^n}{m + m_a}, \tag{17}$$

$$\dot{y}^{\,n+1} = \dot{y}^{\,n} + \Delta t\, \ddot{y}^n, \tag{18}$$

$$y^{\,n+1} = y^{\,n} + \Delta t\, \dot{y}^{\,n+1}. \tag{19}$$

3 ANALYSIS

An adaptive time stepping method and Courant-Friedrichs-Lewy condition [Ref. 5] $\mathbf{CFL} = 0.5$ is used to restrict Δt and increase numerical stability. A Reynolds number of $\mathbf{Re} = 100$ is used and a density of $\rho = 1.0$ with initial velocity profile of 0 everywhere except an inflow horizontal velocity of $1.0 m/s$

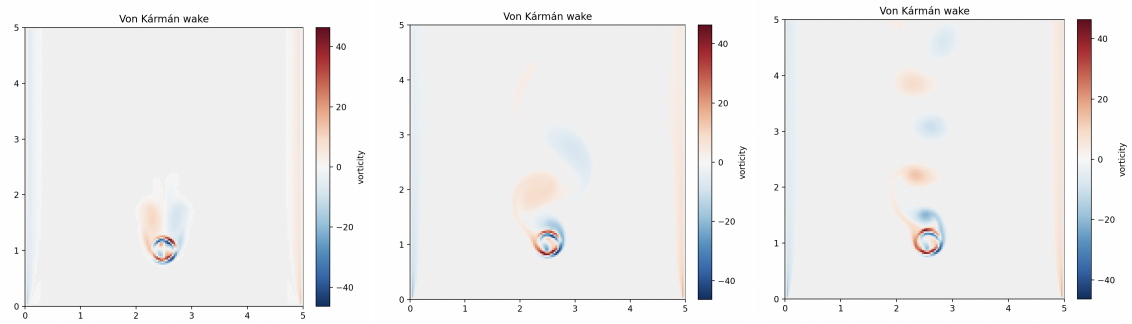

Snapshots of vortex shedding evolution. Counter-clockwise rotating vortices are shown in blue, while clockwise rotating vortices are shown in red.

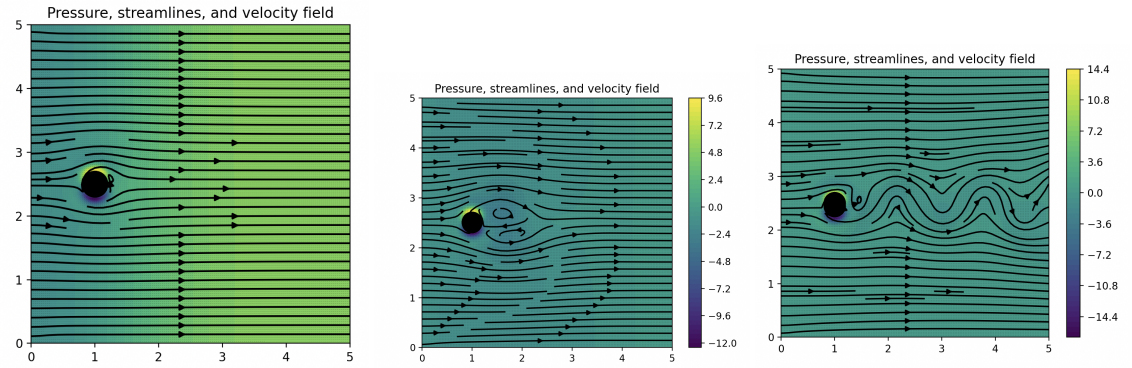
Pressure, streamlines, and velocity field
Pressure, streamlines, and velocity field
Pressure, streamlines, and velocity field

Streamlines representing the velocity flow of the fluid. Pressure gradient is colored in the background.

Results exhibit the expected vortex behavior of Von Karman street. Flow is briefly laminar before separation around the bluff body occurs, leading to low pressure zones shown in purple and high pressure zones shown in bright yellow that induce a suction force on the body. Periodic and alternating suction zones oscillate the cylinder in the fluid, which creates a more turbulent vortex shedding pattern.

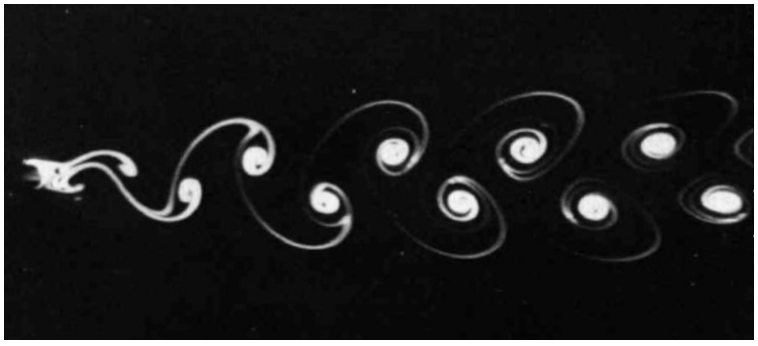

Photography of the Von Karman street at Reynolds number $\mathbf{Re} = 105$. [Ref. 10]

The vortex shedding frequency is calculated by using a statistical method [Ref. 2] that computes the correlation coefficient between fluid flow velocities at each time step:

$$c'_{t,t+1} \equiv A \, \frac{\overline{w_t w_{t+1}}}{\left(\overline{w_t^2}\,\overline{w_{t+1}^2}\right)^{1/2}}, \qquad A = \frac{\min\left(\overline{W_t}, \overline{W_{t+1}}\right)}{\max\left(\overline{W_t}, \overline{W_{t+1}}\right)}. \tag{20}$$

where A is a correction factor and W_t is the magnitude of the flow velocity at time t. This yields a raw signal of the correlation coefficient vs time:

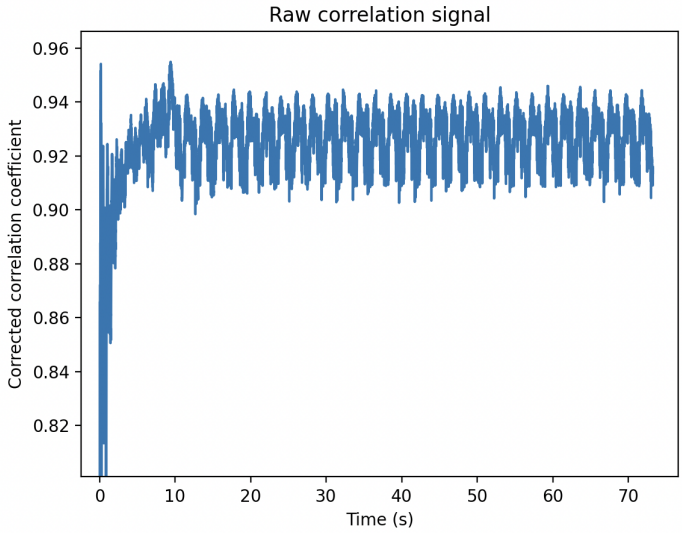

Fluid flow velocity is highly correlated from one time step to another, which matches physical expectation.

The raw correlation signal $\mathbf{c_{raw}}$ is then subtracted from its mean to normalize fluctuations near 0. This new signal is represented as $\mathbf{c}*$. The Fast Fourier Transform requires uniform bin sizes, yet we have implemented an adaptive time-stepping scheme to solve the 2-D Navier Stokes equation. A signal $\mathbf{c_{processed}}$ is created by interpolating $\mathbf{c}*$ onto a uniform time array with sampling frequency $F_s = 20$ Hz. Finally, $\mathbf{c_{processed}}$ is linearly detrended to reduce drift and a Hanning window function is applied to smooth out noise at end points:

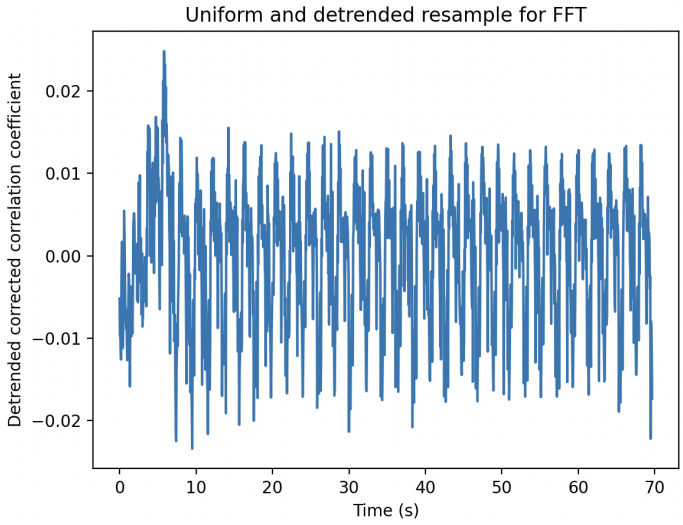

Post-processed correlation signal

Performing a power spectrum analysis of the processed signal $\mathbf{c_{processed}}$ yields the following Fast Fourier Transform:

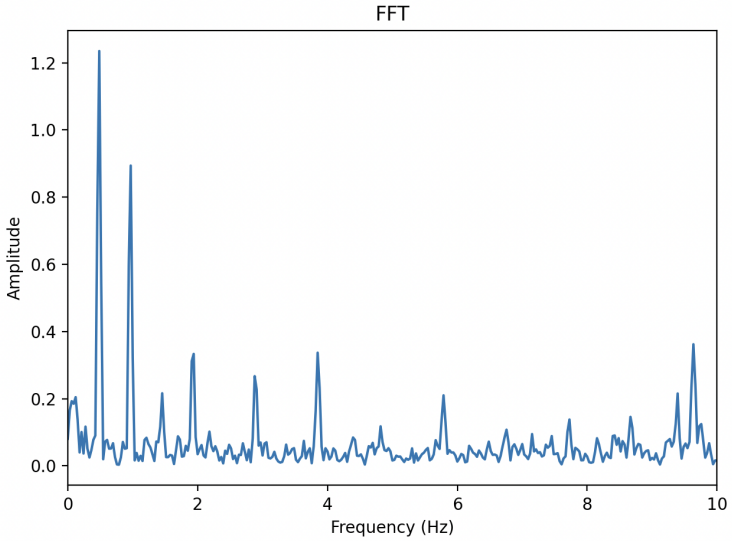

Scanning the peaks yields a shedding frequency of $f = 0.4878$ Hz. Calculating the dimensionless Strouhal number:

$$St = \frac{fL}{U}, \tag{21}$$

where f is the shedding frequency, L is the cylinder diameter (characteristic length), and U is the free-stream velocity of 1.0 m/s. This yields a Strouhal number of 0.1951. The accepted Strouhal number for Reynolds number $\mathbf{Re} = 100$ over a cylindrical bluff body is 0.173; thus our error margin is $+0.0221$ over the accepted value [Ref. 1].

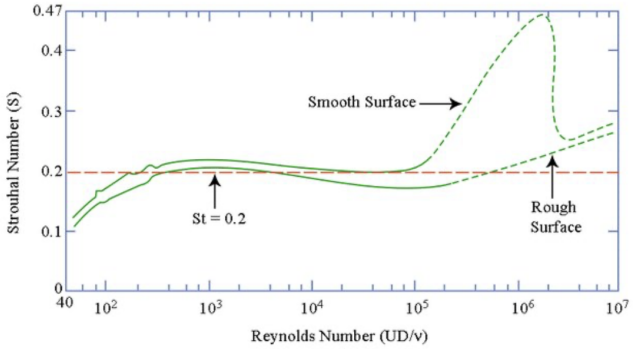

Relationship between Reynolds number and Strouhal's number for uniform free stream flow over cylinders [Ref. 1].

By attaching a magnet to one end of the cylinder and driving it in and out of a coil of wire, one can generate power through the Faraday's law of electromagnetic induction. The induced current also drives a back EMF onto the cylinder, which dampens the oscillations and must be incorporated into the cylinder's equations of motion. This damping force is calculated [Ref. 3] via:

$$\mathbf{F_m}^n = \zeta g^2 \dot{y^n} \tag{22}$$

where $\zeta = \frac{{\mu_m}^2}{R_{load} D^4}$ is the electromagnetic damping coefficient computed from the magnetic moment $\mu_m = 0.2$ Am^2, net resistive load $R_{load} = 10\Omega$, cylinder diameter D and g is the following non-linear function:

$$g = \left(\frac{2\pi N a^2}{L}\right)\left[\frac{1}{(a^2 + (y_{cm} - L/2)^2)^{3/2}} - \frac{1}{(a^2 + (y_{cm} + L/2)^2)^{3/2}}\right]. \tag{23}$$

where $N = 100$ number of turns of the coil, $L = .1$ m is the length of the conducting wire, $a = .05$ m is the radius of the conducting wire, and $y^n_{cm} = 1 + y^n$ is the distance of the magnet from the coil. The time-dependent electrical power generated is

computed by:

$$P(t) = \mathbf{F_m}\dot{y} \tag{24}$$

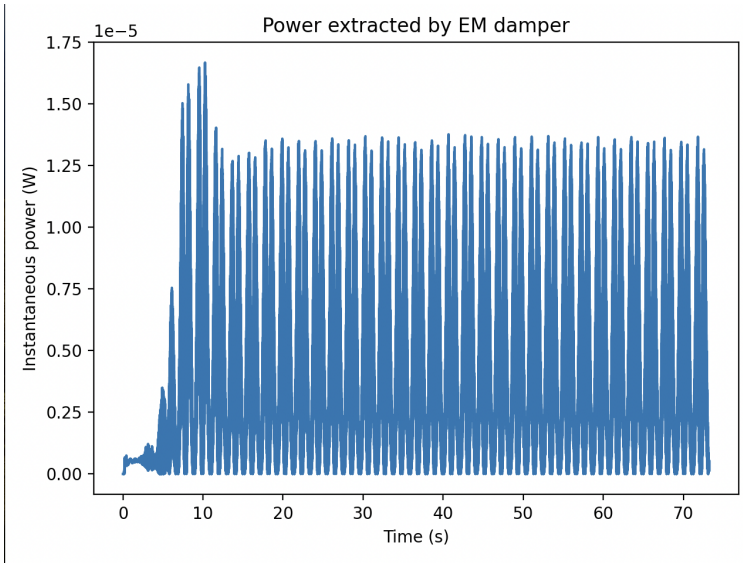

Extracted power in micro-watts versus time via Faraday's law

The average power generated by the cylinder is given by:

$$\frac{1}{T}\int_T P(t)dt \tag{25}$$

which yields us $4.122 * 10^{-6}W$ or $4.122\mu W$. Current published works [Ref. 3] suggests that average power generated via VIV-driven electromagnetic induction by small cylinders is in the several microwatts, which is what corroborates what is seen in our preliminary results.

4 CONCLUSION

A numerical algorithm for solving the incompressible 2-D Navier Stokes equation was developed, which successfully showcases typical vortex shedding behavior at low Reynolds flow and predicts Strouhal number consistent with published data on cylindrical boundary flow. Preliminary results suggest power generation for a singular thin cylinder of radius 0.2m and 1 kg of mass can produce power in micro watts in 2 knots of inflow current. Prior research has found that power generation on the micro watt scale is expected, but improving numerical stability of the Navier-Stokes solver to handle a greater computational domain is necessary to match exact parameters used in experimental data for power generation. This can be done by increasing grid resolution and using a body-fitted curvilinear mesh. This will inevitably require more time iterations and computational power to solve the Navier-Stokes equation. The greatest benefit of a VIV-powered generator is that scaling up only requires implementing more cylinders, which in theory should multiply the power output and provide ecologically safe and renewable energy.

5 ACKNOWLEDGEMENTS

The author thanks Professor Duncan Carlsmith of the University of Wisconsin-Madison for his mentorship, providing guidance and direction through challenges faced in this project. This work was completed to fulfill requirements for The UW-Madison course Physics 499, Fall 2025.

6 SUPPLEMENTAL INFORMATION

The code for this paper can be found on GitHub: https://github.com/sundarramdatla/Power-Generation-via-Vortex-Induced-Vibrations.git. A domain 5x5 computational domain with 161 Eulerian grid points was used for this simulation. The simulation uses 20,000 iterations of the algorithm developed and 50 iterations for the Jacobi iterations at each time step, corresponding to approximately 1 minute and 20 seconds in real time. An adaptive time stepping scheme is used:

$$\Delta t_{visc} = CFL\frac{\Delta x}{\nu}, \qquad \Delta t_{conv} = CFL\frac{\Delta x}{\mathbf{w}_{max}}, \tag{26}$$

The step size Δt is calculated at each time step as the $\min(\Delta t_{conv}, \Delta t_{visc})$ for increased numerical stability by ensuring that the temporal step size does not exceed the grid spacing. Total run-time for simulation is 4 minutes and 44 seconds.

REFERENCES

[1] M. A. Mendez, M. D. Nardo, and C. Benocci, "Running FineOpen43 Simulations at VKI: A tutorial and a collection of scripts," Von Karman Institute for Fluid Dynamics, Technical Report, 2017.

[2] L. Wang, Y. Wang, and Z. Li, "A method to estimate vortex shedding frequency in turbulence," in *Proceedings of the 3rd International Congress on Image and Signal Processing (CISP 2010)*, vol. 5, pp. 3386–3390, 2010.

[3] A. K. Soti, M. C. Thompson, J. Sheridan, and R. Bhardwaj, "Harnessing electrical power from vortex-induced vibration of a circular cylinder," *Journal of Fluids and Structures*, vol. 70, pp. 360–373, 2017.

[4] L. A. Barba, "CFD Python: 12 steps to Navier–Stokes," 2013. Online: `lorenabarba.com`.

[5] G. Caminha, "The CFL Condition and How to Choose Your Timestep Size," SimScale Blog, 2017. Online: `simscale.com`.

[6] S. Gsell and J. Favier, "Direct-forcing immersed-boundary method: A simple correction preventing boundary slip error," *Journal of Computational Physics*, vol. 435, 110265, 2021.

[7] H. Bandringa, *Immersed Boundary Methods*, 2010, pp. 15–18.

[8] R. Pelaez, "Immersed Boundary Method — UAMMD 2.0 documentation," 2016. Online: `readthedocs.io`.

[9] University of Michigan News, "Tech Startup Bets on Slow Water to Power Our Future," 14 Sept. 2016. Online: `news.umich.edu/tech-startup-bets-on-slow-water-to-power-our-future/`

[10] Wikipedia Contributors, "Kármán Vortex Street," 29 Sept. 2020. Online: `en.wikipedia.org/wiki/K%C3%A1rm%C3%A1n_vortex_street`.